Journal of the European Ceramic Society 22 (2002) 2133–2142

www.elsevier.com/locate/jeurceramsoc

Microstructural modifications of ferroelectric lead zirconate titanate ceramics due to bipolar electric fatigue

Jürgen Nuffer[a], Doru C. Lupascu[a], Alexandre Glazounov[b], Hans-Joachim Kleebe[c], Jürgen Rödel[a,*]

[a]*Darmstadt University of Technology, Institute of Materials Science, Petersenstr. 23, D- 64287 Darmstadt, Germany*
[b]*Institute for Ceramics in Mechanical Engineering, University of Karlsruhe, Haid-und-Neu Str. 7, D-76131 Karlsruhe, Germany*
[c]*Bayreuth University, Institute for Materials Research, Ceramics and Composites Group, Ludwig-Thoma Str. 36b, D-95447 Bayreuth, Germany*

Received 26 October 2001; accepted 29 December 2001

Abstract

Fatigue in ferroelectric ceramics is the result of an intricate interplay of electrical, mechanical and electrochemical processes, each of which has been claimed responsible for fatigue. We present experimental results interrelating the different scales of the fatigue mechanism showing that all forms of fatigue occur. Electrochemical mechanisms lead to point defect agglomeration. The agglomerates are rendered visible as etch grooves in strongly etched surfaces by scanning electron microscopy. The overall length of the etch grooves strongly increases during cycling. Micro- and macrocracking were both observed and quantified using electron and optical microscopy. Their number similarly increases as a result of fatigue. Furthermore, a shrinkage of the unit cell volume was found by XRD.

Keywords: Crack growth; Electron microscopy; Fatigue; Ferroelectric properties; PZT

1. Introduction

Two major applications for ferroelectric materials are non-volatile ferroelectric memories[1] and piezoelectric actuators.[2] In each case, fatigue has been addressed as a major obstacle to the transfer of ferroelectric devices from niche applications into mass consumer markets.

Fatigue occurs, when the repetitive application of external loads changes the properties of the material or device. In most actuator applications unipolar electric fields are applied to the material taking advantage of the piezoelectric effect of a poled ceramic. In memory applications the polarisation of the material has to be reversed to provide a permanent change of the material state and thus a remnant unit of information. Therefore, bipolar fields are applied to memory devices. The mechanisms of device and material degradation are still unclear. Some may occur in both cases, some only under unipolar or bipolar driving conditions, some only in thin films, others only in bulk material.

Actuator applications take advantage of the piezoelectric coupling converting electrical into mechanical energy. This property is used in multilayer actuator devices for fuel injectors and adaptronics, in ultrasound sources, or in ultrasonic motors.[2–4] Even though the devices are generally driven at unipolar fields, certain parts of the device may experience mixed electromechanical loading.

The present investigation deals with bipolar fatigue of ferroelectric bulk ceramics to understand the underlying fatigue mechanisms. Bipolar fatigue shows the most pronounced fatigue effects and may be considered an accelerated device test to some extent. Under bipolar driving, ferroelectric materials show a reduction of the macroscopic polarisation and strain after a certain amount of switching cycles[5–10] ranging from as few as 20 [11] to 10.[9] [12] The fatigue rate depends on several factors, such as the composition of the ceramic,[13] the type of electrodes[12] temperature,[13,14] the mechanical boundary conditions[15], frequency[16] and amplitude[17] of the cycling field. Despite the large number of works in this field a comprehensive understanding of fatigue has not been achieved yet.

Fairly high agreement exists that the primary cause of fatigue is related to the dynamics of point defects.[1,6,10,18–22] In the framework of this general agreement, several forms

* Corresponding author. Tel.: +49-6151-166315; fax: +49-6151-166314.
E-mail address: roedel@ceramics.tu-darmstadt.de (J. Rödel).

0955-2219/02/$ - see front matter
PII: S0955-2219(02)00017-1

may arise, formation of space charges at grain boundaries or electrodes,[11] formation of defect dipoles and their orientation within the ferroelectric domains,[23,24] or the agglomeration of point defects to larger hard agglomerates.[6,10] In any case, either the overall degree of polarisation or the amount of switchable polarisation are reduced. This in turn reduces the effective piezoelectric coefficient of the ceramic.[2] About 80% of the lost polarisation can be restored by thermal treatment well above the Curie temperature,[25] which implies the re-distribution of agglomerated defects at high temperatures and directly supports an electrochemical mechanism. Hard agglomerates have been hypothesised in several publications,[6,18–20,22] and were rendered visible in a recent work.[10]

We recently refuted the long standing hypothesis,[7] that significant amounts of oxygen escape from bulk ceramic lead zirconate titanate (PZT) during bipolar electric cycling.[25] The massive amount of oxygen liberated at this moment generating the corresponding amount of vacancies in the ceramic was considered the primary cause for a reduction in switchable polarisation. The oxygen liberation was assumed to be the first step in the damage scenario laying ground for all the following steps like point defect agglomeration and unit cell shrinkage. On the other hand, it has recently been discussed that the number of point defects introduced during processing is sufficient to provide the agglomerate growth.[22] Exchange of oxygen with surrounding atmospheres is only relevant in thin films.[9] It has to be kept in mind throughout this text, that all material changes arise without exchange of oxygen with the external atmosphere.

The second major effect of fatigue is the formation of microscopic and macroscopic cracks. These lead to the reduction of the electric field in the bulk ceramic, and hence necessitate higher external fields for polarisation switching.[26–28] The formation of microscopic cracks with a typical length of a few hundred nanometers may be responsible for reduction of polarisation switching as suggested by FEM results,[29] and recently supported by experimental data.[30] However, the role of crack formation in the overall problem is still unclear. In particular, the question whether microcracks are a result or the cause of fatigue remains open.[31] Macroscopic cracks are able to reduce the effective electric field in the vicinity of some grains in a similar sense.[32]

A phenomenological study on the fatigue behaviour of the commercial PZT ceramic PI 151 was recently presented.[10] In the present paper the authors demonstrate the formation of defect agglomerates and microcracks of different forms and locations in the microstructure during cyclic fatigue as well as effects on the size of average unit cells. Different length scales reaching from macroscopic cracks of several mm in length down to unit cell dimensions of point defects are covered.

2. Experimental

2.1. Samples

The measurements are performed on a commercial PZT material (PIC 151, PI Ceramic, Lederhose, Germany) of composition $Pb_{0.99}[Zr_{0.45}\ Ti_{0.47}\ (Ni_{0.33}\ Sb_{0.67})_{0.08}]O_3$. The samples are disc shaped with 10 mm in diameter and 1 mm thickness. Silver electrodes are burnt into the surfaces at 850 °C, leaving a rim of approx. 250 μm uncovered to avoid arcing. All samples are poled by the manufacturer with 2.5 kV/mm for 1 min at room temperature. The mean grain size is approximately 6 μm,[33] the coercive field determined from quasistatic measurement of polarisation hysteresis loops is $E_C = 1.03$ kV/mm,[10] and the Curie temperature approximately 250 °C.[25]

2.2. Cycling

The samples are damaged by cycling with sinusoidal electric field of 1.96, 1.4 or 1.0 kV/mm amplitude, which corresponds to about 2, 1.4 and 1.0 E_c. Details of the cycling procedure can be found in Ref. 10 and are only briefly outlined here. The samples are placed between two metal clamps serving as electrical contact. The setup is immersed in silicone oil (Wacker, Germany) to avoid arcing and to guarantee heat transfer during cycling. The cycling voltage was applied such that the peak field is increased within 5 s to the desired maximum field and held constant for N cycles. Then the field is decreased again within 5 s leaving the sample with negligible remnant polarisation ($P \approx 0$). Between cycling and further treatment a waiting time of 4 h was introduced, mainly to cool the sample to room temperature and restrain all aging effects to the same time interval.

2.3. Macroscopic polarisation

The macroscopic polarisation of cycled samples was measured by means of a capacitor placed in series with the sample. The capacitor integrates the current during application of a triangular bipolar voltage of 0.02 Hz and 2 kV/mm amplitude. The voltage on the capacitor was measured using an electrometer (Keithley; input impedance $10,^{14}$ Ω). The data were collected by an analogue-digital converter.

2.4. Etch grooves

Chemical etching is used to visualise the etch grooves.[10] It was observed in previous studies that fatigue may be highly anisotropic.[34] Thus, the orientations of the cross sections under investigation are relevant. Different from the samples in Ref. 10 cross-sections *perpendicular* to the electrodes are displayed in the present study. Rectangular bars were cut from the disc

shaped samples and polished on the 1×10 mm^2 surface. The polished surfaces were etched with a drop of acid containing a mixture of HF/HCl. The acid drop was rinsed off intensively after 60 s using distilled water. For SEM investigation a thin layer of Au/Pd was sputtered onto the samples.

All scanning electron microscopy (SEM) investigations are performed in secondary electron mode at a magnification of 4000 times (XL30 FEG, Philips, Netherlands). 17 pictures of 60×40 μm^2 are taken in a row across the thickness direction of each sample. For each picture, the etch groove length is determined by a software fitting linear line elements to the etch pattern on the image (LINCE[35]). The software adds the lengths of all line elements to obtain a total length. This value is plotted against the position of the picture on the cross section.

2.5. X-ray diffraction

Measurements of X-ray diffraction (XRD) from both virgin and fatigued samples were performed using synchrotron radiation at the G3 beam station of HASYLAB (DESY, Hamburg). The diffractometer available at this station has a position sensitive detector, which consists of a CCD camera and a multi-channel plate placed between the camera and the sample.[36] The plate consists of a large number of parallel tubes, each with 10 μm in diameter. When a wide parallel X-ray beam irradiates the sample surface, each tube selects diffracted radiation from a small spot on the sample and directs it to the CCD camera. The output signal from the camera is an image corresponding to the distribution of diffracted intensity over the sample surface area. In the present experiments, each point in the image corresponds to a spot on the sample surface with dimensions approximately equal to 15×15 μm^2.

X-ray diffraction was measured from the polished cross-section surface of the samples. In order to avoid possible errors related to the uncertainty of the determination of the wavelength, the measurements were performed simultaneously on the virgin and fatigued samples. The samples were glued to the glass plate next to each other, and the plate was subsequently mounted in the diffractometer. The wavelength of the synchrotron radiation was equal to $\lambda=0.15395$ nm.

The material studied, PIC-151, is a tetragonal ferroelectric modification. To determine a possible variation of lattice parameters c and a across the sample thickness, XRD was measured around (002)/(200) reflections. The scans were performed using θ–2θ mode. At each diffraction angle θ, an image corresponding to a spatial distribution of diffracted intensity over the polished surface was recorded by the CCD camera of the detector. The intensity was subsequently integrated to increase the signal-to-noise ratio. Integration was performed in each image within the regions across a width equal to the width of the sample (in the direction along the electrodes) and a length equal to 50 μm (in the direction of the sample thickness). After integration the averaged intensities were plotted as a function of the diffraction angle θ, at different distances from the electrode surfaces. The lattice parameters c (from θ_{002}) and a (from θ_{200}) were calculated from the positions of the diffraction peaks, θ_{002} and θ_{200}.

2.6. Transmission electron microscopy

A fatigued sample (10^8 cycles, 1.96 kV/mm) and an unfatigued sample were prepared for TEM observation as follows. A cylinder of 3 mm in diameter was extracted from the sample by means of an ultrasonic drill. It was ground and polished to 100 μm thickness and then dimpled down to 10 μm. Further material was removed by ion thinning. A thin layer of carbon was sputtered onto the sample to avoid charging during transmission electron microscope (TEM) observation. One sample foil was located in the very centre of the sample (5 mm from the edge and 0.5 mm under the electroded surface), another one was taken from the region immediately underneath the electrode at 40–50 μm depth. The samples were investigated by means of a transmission electron microscope (Philips CM20FEG) at 200 kV with a resolution of 0.24 nm. The sample foil was examined at different perforated locations for statistics.

2.7. Macroscopic cracks

Macroscopic cracks were observed in an optical microscope (Leica DM-R). Samples cycled at 1.96, 1.4 and 1.0 kV/mm were investigated at different cycle numbers. Again, rectangular bars were cut from the samples, ground, and polished on the 1 mm$\times$10 mm thickness profile to a 3 μm finish. The region near the sample edges was of particular interest. Pictures were taken along the electroded edges showing the macroscopic cracks. An overall crack length for the whole sample was determined by the same method as the overall etch groove length described above. The sum of crack lengths determined for all pictures taken on the particular sample is the crack length value assigned to the sample. In case of the 1.96 kV/mm cycling field, where the most intensive cracking occurred, two samples were investigated at each cycle number for statistics. In all other cases, one sample was used.

3. Results and discussion

3.1. Macroscopic polarisation

The damage evolution during cycling at three different cycling fields is provided in Fig. 1. The value of

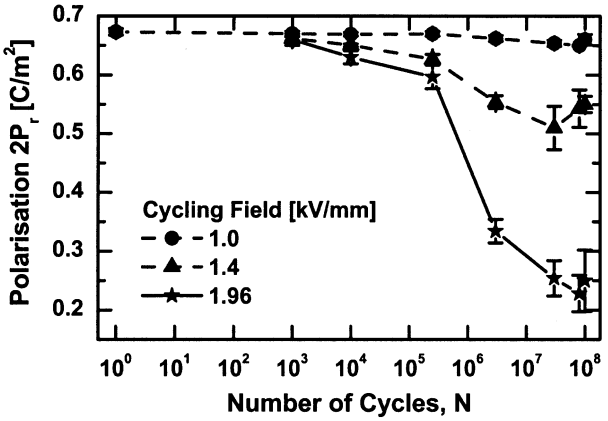

Fig. 1. Evolution of twice the remnant polarisation during bipolar electric fatigue for different cycling fields.[10]

twice the remnant polarisation 2 P_r, is plotted vs. cycle number for cycling voltages 1.0, 1.4, and 1.96 kV/mm. The highest cycling field leads to the strongest fatigue. For 1.96 kV/mm cycling field a decay of polarisation from 0.68 to 0.28 C/m^2 occurs between 2.5×10^5 and 3×10^7 cycles, and after 10^7 cycles no further reduction is observed. Cycling at 1.0 kV/mm does not lead to any fatigue, while cycling at 1.4 kV/mm leads to an intermediate fatigue rate. The macroscopic fatigue behaviour of this material is in good agreement with other studies.[34,37]

3.2. Etch grooves

In Fig. 2 the etched surfaces of a fatigued sample are shown. Fig. 2a displays the region near the electroded surfaces, while Fig. 2b depicts a region in the centre of the sample (500 μm from the electrodes). The latter shows a structure which we call etch grooves is the following. Several grains are interspersed by etch grooves of approx. 1–5 μm in length. The fact that etch grooves are visible in fatigued samples shows that chemical properties of the sample change locally during cycling, leading to a changed affinity to the attacking acid. This assumption is supported by the observation that shorter etching times and smaller acid drops do not reveal the etch grooves.

In our previous study,[10] we already interpreted these etch grooves as a direct image of the defect agglomerates which are suggested to be present in cycled samples and mainly responsible for the observed fatigue. The point defects involved are most probably oxygen vacancies, since they are the most mobile defects in perovskites at room temperature.[38,39]

Since we recently found that the overall amount of the oxygen vacancies does not change during cycling,[40] this amount solely depends on the dopant concentration and the vacancies frozen in during cooling from the sintering process. If antimony ions used for soft doping are of valence +5, then one would expect no oxygen vacancies

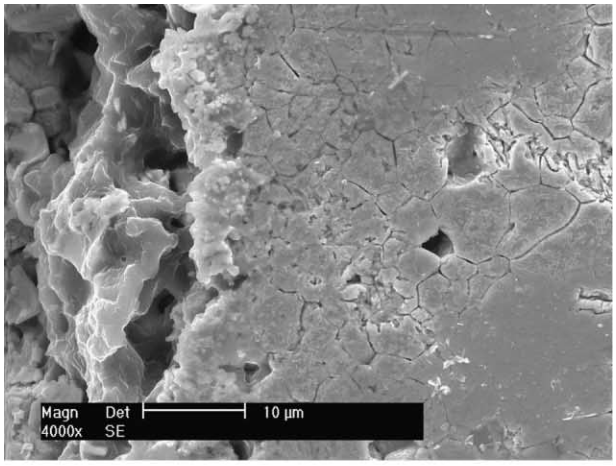

(a)

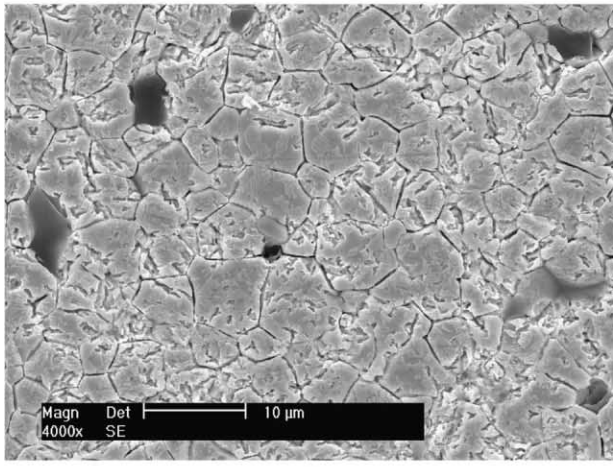

(b)

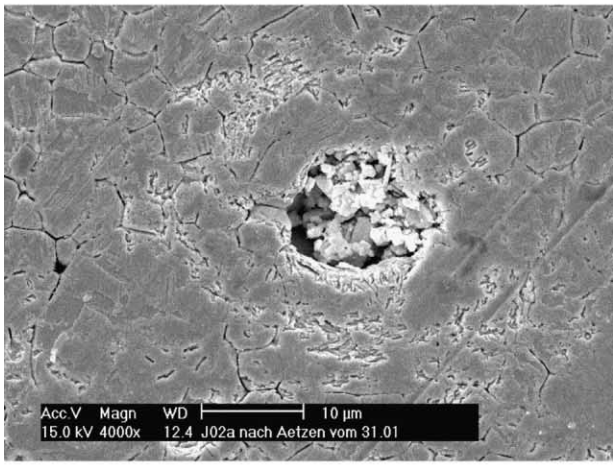

(c)

Fig. 2. Images of etch grooves observed by scanning electron microscopy on the surfaces of fatigued samples: (a) microstructure near the electrode (strongly etched on the left). First etch grooves visible in the upper right corner of the image to the right of the pore, (b) etch grooves in the middle of the sample, 500 μm distant from each electrode, (c) etch grooves in the vicinity of a pore.

to be present. When we assume antimony to be of valence +3, we obtain an oxygen vacancy concentration of 1.3%,[40] of all available oxygen ions. This concentration is largely sufficient to provide enough point defects for the formation of extended hard agglomerates observed in this study.

Fig. 2c presents a peculiarity of etch grooves forming a ring shaped structure around a pore. The grooves are obviously preferably located near that pore rather than at a certain distance. That gives further support to the assumption that the etch grooves observed here are caused by point defect agglomeration. Under electromechanical load, a pore is known to serve as a concentrator of mechanical stresses and electric fields. Additionally, since PZT material is missing in the interior of a pore, there is also a concentration gradient of point defects. Consequently, there are large gradients in the chemical potential, high electric fields, and high mechanical stresses around a pore which facilitate the ion motion towards the respective defect agglomerates.

Defect agglomerates like chains or plates do not form in perovskites in thermal equilibrium as long as the concentration of oxygen vacancies is low.[41] In the case of a quenched concentration of oxygen vacancies, which are predominantly highly charged ($V_{\ddot{O}}$), a strong interaction with domains can occur. In a ferroelectric material, the energetic situation on a microscopic scale then becomes distinctly different. By using a simple Landau—type potential Brennan,[6] showed that a configuration consisting of a point defect like an oxygen vacancy located at a tail to tail boundary of two 180° domains leads to a minimised free energy. He showed in a similar line of arguments that the ordering of many point defects in a two-dimensional array is more stable than the stochastic spatial distribution of the defects in the crystal. The enhanced diffusion towards such defect agglomerates will be discussed in a forthcoming paper. The only important message needed here is that once a vacancy is trapped at an agglomerate it will not be released.

The comparison of Fig. 2a with Fig. 2b reveals that there is a gradient in density of these etch grooves. Only few etch grooves are visible very close to the electrode edges, while their number increases with increasing distance from the edge. In the middle of the sample, where the image in Fig. 2b was taken, the density is highest.

In order to show this quantitatively, the etch groove length was plotted along the sample cross section for three cycling stages: 0, 3×10,[6] and 10^8 cycles in Fig. 3. No etch grooves are observed in the uncycled sample. Cycling with 10^8 cycles leads to a profile with its maximum in the centre of the sample. In this region, the overall length per image is 380 μm. The same profile is also observed for cycling up to 3×10^6 cycles, but the overall etch groove length is smaller.

The fact that more etch grooves are observed in a sample cycled up to higher cycle number is easily understood according to the discussion above. With longer cycling time, the defects move longer distances and therefore the probability of forming an agglomerate increases.

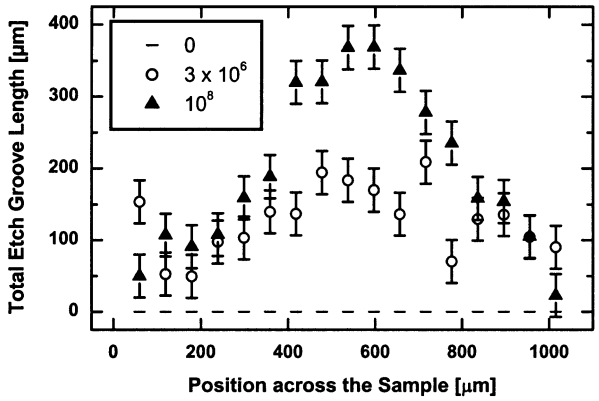

Fig. 3. Total etch groove length per image (40×60 μm) plotted versus position of the image along the sample cross section for cycle numbers 0.3×10^6, 10^8.

On the other hand, the fact that more etch grooves are found in the centre of the fatigued sample is not understood, yet. A possible correlation may be drawn to the fact that we find porous regions near the electrodes not present in the centre of the sample as shown in Fig. 4. In the region of high etch groove density (centre of the sample) no pores at grain boundary triple points are found in TEM images before or after fatigue. In the region of low etch groove density (near the electrodes) the triple points contain a pore after ion thinning. The most likely explanation of this effect is silver migration into ceramic PZT during electrode firing. It is known that silver migration along grain boundaries is three orders of magnitude larger than into bulk grains.[42,43] For the firing conditions in our samples the mean penetration depth for silver along grain boundaries is 11 μm according to the diffusion coefficient given by Slinkina et al..[42,43] Thus, some silver will have penetrated into the grain boundaries at 40–50 μm depth. This will locally modify the chemistry of the grain boundary and weaken it so that the triple points can be thinned out during ion thinning. This may also be the reason for finding some amorphous material at the triple points only after fatigue and only in the near-electrode regions.

3.3. X-ray diffraction

From the lattice parameters c and a of the tetragonal phase determined from the X-ray diffraction measurements the volume of the unit cell was calculated: $V=c\,a^2$. Fig. 5 shows the unit cell volume determined at different points across the sample thickness. The average volume is smaller in case of the cycled sample showing an average value of 66.46 Å^3, while in the unfatigued sample it is 5% lower (66.81 Å^3). The reason for this

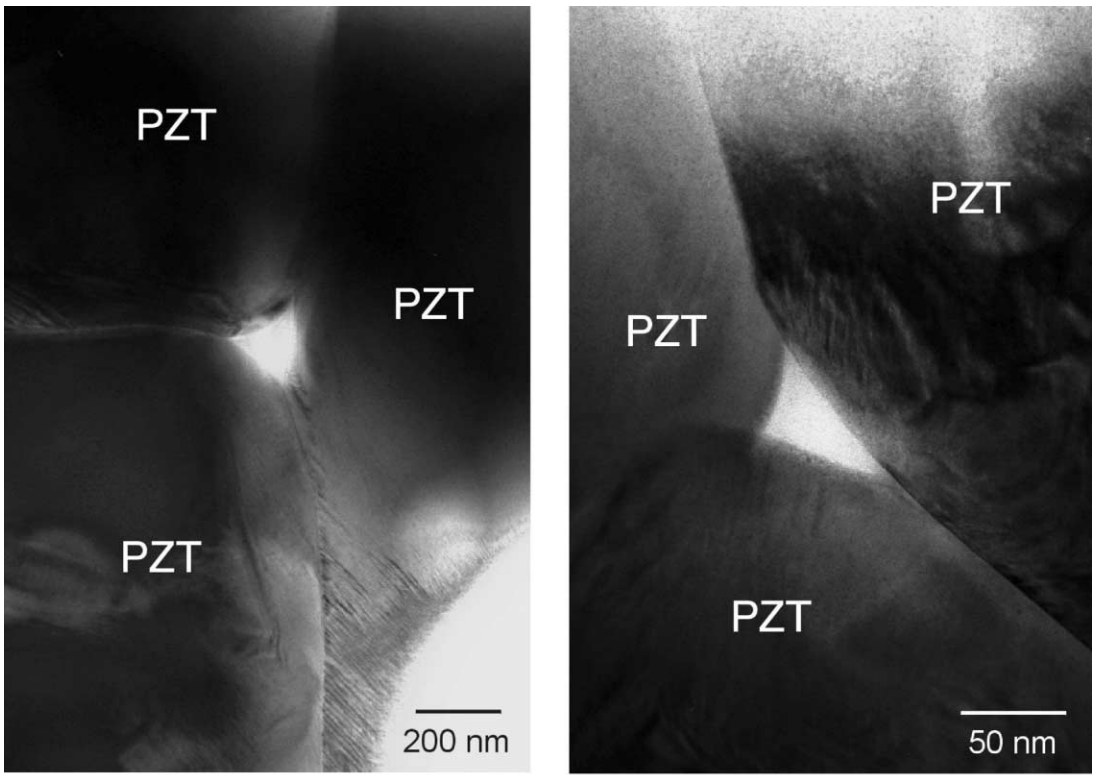

Fig. 4. (a and b) Pores at triple points are found in fatigued samples near the electrodes.

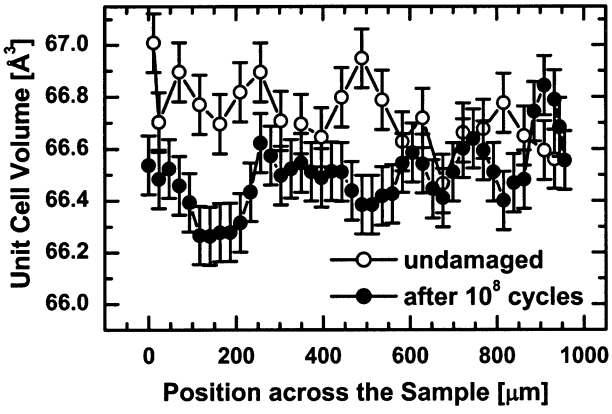

Fig. 5. (a and b) Unit cell volume plotted versus position along the sample cross section for an unfatigued and a fatigued sample (10^8 cycles, 1.96 kV/mm).

reduction is not entirely clear to our understanding. A possible explanation stems from the following observation. Measurements by Kamiya,[44] showed that an increased amount of acceptor doping in the lattice will reduce the c/a ratio irrespective of acceptor type. We observed that a darkening of the samples occurred during cycling and it approached colours of hard doped materials. Thus, the number of acceptor centres may increase and reduce the c/a ratio. A possible candidate is the lead ion, because darkening under UV illumination or fatigue has been observed for many soft- doped materials and been assigned to recharging of the Pb^{3+}- ion.[45]

3.4. Microcracking

TEM observations were performed at two different regions of the sample. Fig. 6 shows representative images of the microcracks observed in samples fatigued to 10^8 cycles. The pictures were taken in the centre of the sample. Some microcracks were also found near the electrodes. Unfatigued samples were investigated as well to find out to what degree the observed microcracks in fatigued samples are solely due to the cycling procedure. Microcracks indeed were found in unfatigued samples, but much less in number.

The details of the microcrack initiation process are still unclear in the literature. This holds for ferroelectrics as well as for other ceramics. In the previous section we discussed the shrinkage of the unit cell during cycling as one possible origin of microcracking, but this is rather speculative and is not directly supported by experimental evidence. Therefore, the following discussion is solely focused on the question what consequence a given microcrack density has on the polarisability of the sample.

It is widely accepted that electrochemical mechanisms play a dominant role in the fatigue phenomena. However, mechanical mechanisms like microcracking may not be underestimated. In our material, we previously

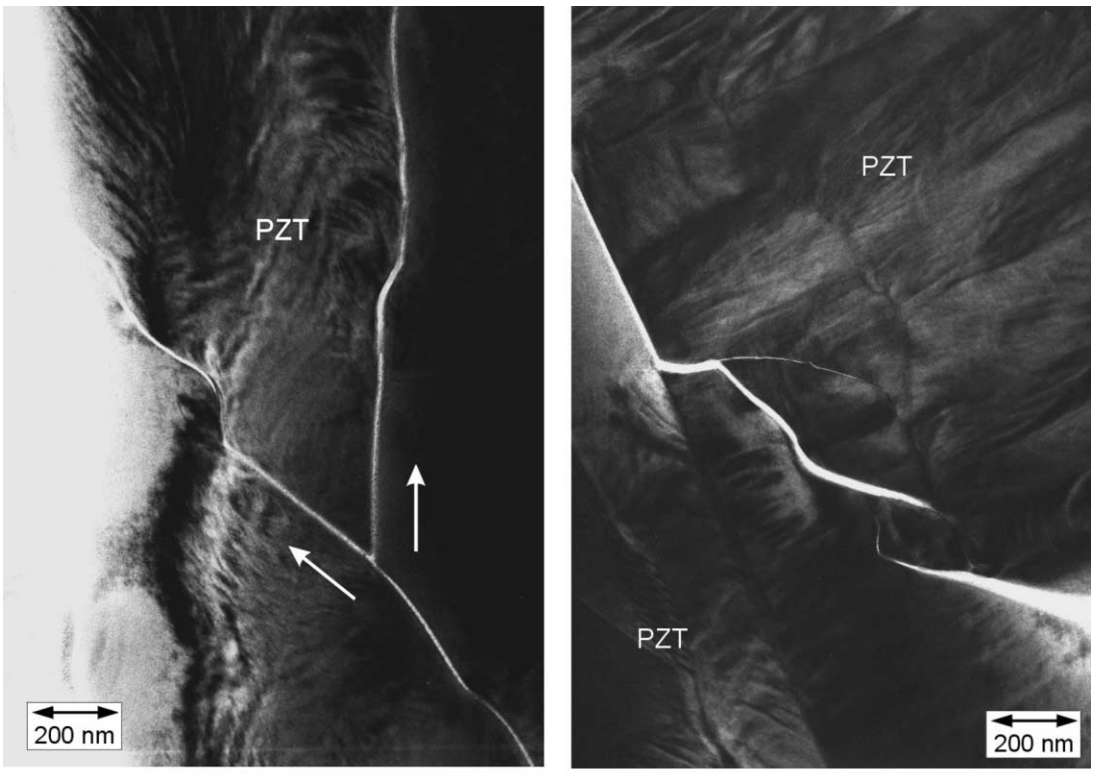

Fig. 6. (a and b) Two representative images of microcracks. The pictures were taken in the centre of a fatigued sample (500 μm from the electrodes).

found,[25] that thermal annealing of fatigued samples up to 700 °C can recover about 80% of the lost polarisation, while the remainder of 20% is attributed to some form of permanent damage. Microcracking is a possible source for the reduced switchability of domains as already discussed in the introduction. The relevance of microcracking was previously demonstrated for transparent electrostrictive PLZT where a good correlation between the microcrack density and the reduced polarisation was found.[30] These data confirm the numerical simulation of the effect of microcracks on the macroscopic polarisation by Kim et al..[29] It is, therefore, important, but unfortunately very difficult in opaque samples to determine the existence of microcracks experimentally. In our present study, TEM observations performed with sufficient statistics confirmed that there is an enhanced microcrack density in fatigued samples. We conclude that fatigue non recoverable by thermal treatment is at least partially due to the existence of micro- and macrocracks.

3.5. Macrocracking

Fig. 7 shows the overall appearance of the macroscopic crack pattern. The location of the image on the sample cross section is shown. Two different types of cracks were observed: (1) edge cracks, which started at the boundary between electroded (and therefore piezoactive) and unelectroded (inactive) material. (2) Delamination cracks which appeared underneath the electrodes and propagated predominantly parallel to the electrodes.

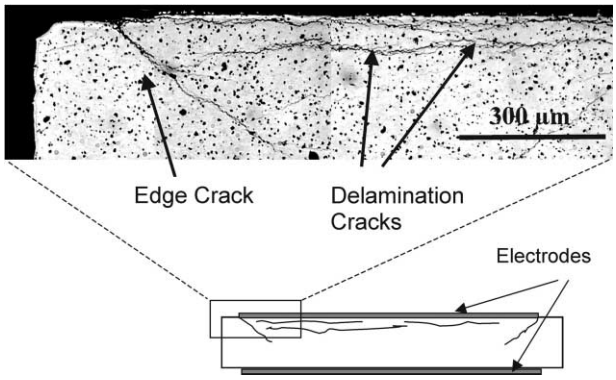

Fig. 7. Macroscopic crack pattern observed by optical microscopy. The schematic drawing shows the overall appearance of the cracks and the location of the above image.

In each sample the crack pattern only appeared at one electrode. The side varied from sample to sample with respect to the reference electrode. Secondly, the crack pattern only appeared for cycling with 1.96 kV/mm and for high (greater 10^5) cycle numbers. In all other cases, only a few distinct cracks were observed.

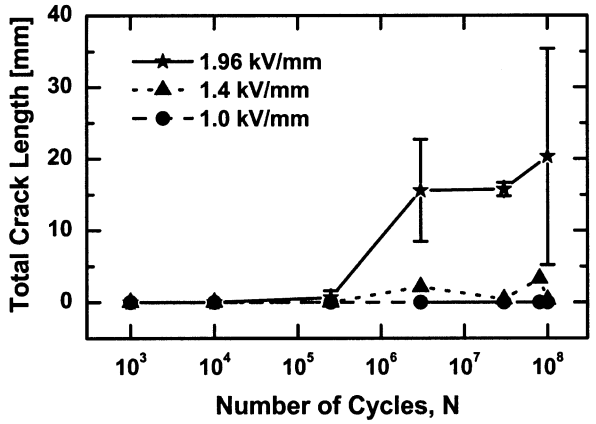

Fig. 8. Crack length plotted versus cycle number for three different cycling fields.

The evolution of the macrocrack length for the three different cycling fields 1.0, 1.4 and 1.96 kV/mm is shown in Fig. 8. For 1.0 kV/mm, no fatigue occurred, while cycling at 1.4 kV/mm leads to comparably small crack lengths of approx. 3 mm at cycle numbers greater than 2.5×10^5. The cracks observed for this cycling field are solely constituted of edge cracks. No delamination was observed in this case. Cycling at 1.96 kV/mm leads to severe cracking for high cycle numbers. Several layers of cracks developed during cycling. It is of interest that there is no cracking for $N<3\times10^6$ cycles, i.e. before the major drop in switchable polarisation occurs (see Fig. 1), while for cycle numbers greater than 3×10^6 a saturation value of approx. 18 mm is reached.

It is known that cracks, once initiated by Knoop- or Vickers indentation propagate preferably parallel rather than perpendicular to the electrodes.[32,37,46,47] The reason for this anisotropy is not well understood. Cao and Evans[32] argue that the strain incompatibility between the decreased piezoactivity of the material underneath the crack front and the unchanged piezoactivity of the material beyond the crack tip is responsible for that phenomenon. Weitzing et al.[37] measured the crack length and the ferroelectric strain. They found that after 10^6 cycles the crack extension as well as the degradation of the strain are in saturation and showed no further changes for higher cycle numbers. They concluded that the decrease of strain results in a decrease of the driving force for crack propagation. For cycling at 1.96 kV/mm, this is in good agreement with our observation, since in our case the strain has decreased to its final value after 3×10^6 cycles,[10] and the crack length saturates also.

The just mentioned publications deal with the propagation of cracks, which are already initiated. In our case where no indentation is used, it is important to inquire into the mechanisms that lead to the initiation of the cracks. It is well known that obvious defects like pores[48] or surface unevenness[49] serve as starter flaws for macroscopic cracks. In this work it was not observed that cracks start at those defects. Another plausible argument is that the cracks start at the surfaces and grow perpendicular to the electrodes at an early stage of cycling. Later on they deflect by 90° and grow parallel to the electrodes. This phenomenon was observed by Lucato[15] at partially electroded samples, induced by a strain incompatibility.

The fact that cycling at 1.4 kV/mm only results in edge cracks but not in delamination cracks gives an important additional information. The delamination cracks can only be initiated in case that sufficiently high electric cycling fields exist and a rather strong fatigue of the bulk material has preceded the crack growth. This may partially be due to the fact, that the switchability of domains in the grains is reduced due to the fatigue effects induced by point defect agglomeration. The reduced switchability of the domain system in certain grains reduces the possible accommodation of local stresses between this non-switching grain and neighbouring grains that will still follow the externally applied electric fields by the movement of their domains. The strain mismatch during polarisation inversion may become very much enhanced, leading to stresses finally sufficient to initiate cracking particularly in the non-switching grains.

In contrast to the delamination cracks, the origin of the edge cracks is quite obvious. Since the electroded material elongates due to the piezoelectric and ferroelastic strain but the unelectroded part does not, high mechanical stresses occur at the boundary between both regions. FEM simulations have revealed that such cracks will experience the highest tensile stresses along conical surfaces in the sample interior.[50]

3.6. A damage scenario

Based on the results obtained so far, we formulate a damage hypothesis as a basis for further investigation. As the first step in the damage scenario it is assumed that the oxygen vacancies present in the material prior to cycling are moved around during cycling until they create the first self- stabilising defect agglomerates. During this cycling regime (up to approx. 10^5 cycles) almost no changes of the macroscopic polarisation switching occur. With further cycling (approx. $10^5<N<10^7$), the strong decrease of the polarisation occurs along with a significant growth of the agglomerates. Macroscopically, the net polarisation experiences the major decrease in this cycling range.[10] The defect agglomerates become visible as etch grooves after intensive etching. Severe domain clamping occurs. The average unit cell volume starts to shrink alongside. Some microcracks form starter flaws for the later observed delamination cracks. The macroscopic cracks lead to an additional reduction of the switchable polarisation by reducing the electric field in the ceramic.

Acknowledgements

The financial support by the Deutsche Forschungsgemeinschaft (lu729/1, Ho1156/3) is greatly acknowledged. The authors thank Jan Reszat and T. Wroblewski for their help with the XRD experiments.

References

1. Scott, J. F., *Ferroelectric Memories*. Springer, Berlin, Heidelberg, 2000.
2. Uchino, K., *Piezoelectric Actuators and Ultrasonic Motors*. Kluwer Academic Publishers, Boston, Dordrecht, London, 1997.
3. Haertling, G. H., Ferroelectric ceramics: history and technology. *J. Am. Ceram. Soc.*, 1999, **82**, 797–818.
4. Uchino, K., Ferroelectric ceramics. In *Materials Science and Technology 11*, ed. R. W. Cahn, P. Haasen and E. J. Kramer. VCH Weinheim, Germany, 1994, pp. 635–677.
5. Desu, S. B. and Yoo, I. K., Electrochemical models of failure in oxide perovskites. *Integrated Ferroelectrics*, 1993, **3**, 365–376.
6. Brennan, C., Model of ferroelectric fatigue due to defect/domain interactions. *Ferroelectrics*, 1993, **150**, 199–208.
7. Pan, M.-J., Park, S. E., Markowski, K. A., Yoshikawa, S. and Randall, C. A., Superoxidation and electrochemical reactions during switching in $Pb(Zr,Ti)O_3$ ceramics. *J. Am. Ceram. Soc.*, 1996, **79**, 2971–2974.
8. Gruverman, A., Auciello, O. and Tokumoto, H., Nanoscale investigation of fatigue effect in $Pb(Zr,Ti)O_3$ films. *Appl. Phys. Lett.*, 1996, **69**, 3191–3193.
9. Brazier, M., Mansour, S. and McElfresh, M., Ferroelectric fatigue of $Pb(Zr,Ti)O_3$ thin films measured in atmospheres of varying oxygen concentration. *Appl. Phys. Lett.*, 1999, **74**, 4032–4033.
10. Nuffer, J., Lupascu, D. C. and Rödel, J., Damage evolution in ferroelectric PZT under bipolar electric cycling. *Acta Mater.*, 2000, **48**, 3783–3794.
11. Colla, E. L., Taylor, D. V., Tagantsev, A. K. and Setter, N., Discrimination between bulk and interface scenarios for the suppression of the switchable polarization (fatigue) in $Pb(Zr,Ti)O_3$ thin film capacitors with Pt electrodes. *J. Appl. Phys*, 1998, **72**(19), 2478–2480.
12. Taylor, D. J., Geerse, J. and Larsen, P. K., Fatigue of organometallic chemical vapor deposited $PbZr_xTi_{1-x}O_3$ thin films with Ru/RuO_2 and Pt/Pt electrodes. *Thin Solid Films*, 1995, **263**, 221–230.
13. Jiang, Q. Y., Subbarao, E. C. and Cross, L. E., Effect of composition and temperature on electric fatigue of La-doped lead zirconate titanate ceramics. *J. Appl. Phys*, 1994, **75**, 7433–7443.
14. Wang, D., Fotinich, Y. and Carman, G. P., Influence of temperature on the electromechanical and fatigue behavior of piezoelectric ceramics. *J. Appl. Phys*, 1998, **83**, 5342–5350.
15. dos Santos e Lucato, S. L., Lupascu, D. C., Kamlah, M., Rödel, J. and Lynch, C. S., Constraint-induced crack initiation at electrode edges in piezoelectric ceramics. *Acta Mater.*, 2001, **49**, 2751–2759.
16. Zhang, N., Li, L. and Zhilun, G., Frequency dependence of ferroelectric fatigue in PLZT ceramics. *J. Eur. Ceram. Soc.*, 2001, **21**, 677–681.
17. Mihara, T., Watanabe, H. and Paz de Araujo, C. A., Polarisation Fatigue characteristics of sol- gel ferroelectric $Pb(Zr_{0.4}Ti_{0.6})O_3$ thin-film capacitors. *Jpn. J. Appl. Phys.*, 1994, **33**(P1/7a), 3996–4002.
18. Yoo, I. K. and Desu, S. B., Fatigue modeling of lead zirconate titanate thin films. *Mater. Sci. Eng. B*, 1992, **13**, 319–322.
19. Yoo, I. K. and Desu, S. B., Mechanism of fatigue in ferroelectric thin films. *Phys. Stat. Sol. (a)*, 1992, **133**, 565–573.
20. Yoo, I. K. and Desu, S. B., Fatigue parameters of lead zirconate titanate thin films. *Mater. Res. Soc. Symp. Proc.*, 1992, **243**, 323–329.
21. Dawber, M. and Scott, J. F., A model for fatigue in ferroelectric perovskite thin films. *Appl. Phys. Lett.*, 2000, **76**, 1060–1062.
22. Scott, J. F. and Dawber, M., Oxygen-vacancy ordering as a fatigue mechanism in perovskite ferroelectrics. *Appl. Phys. Lett.*, 2000, **76**, 3801–3803.
23. Robels, U. and Arlt, G., Domain wall clamping in ferroelectrics by orientation of defects. *J. Appl. Phys.*, 1993, **73**, 3454–3460.
24. Robels, U., Schneider-Störmann, L. and Arlt, G., Dielectric aging and its temperature dependence in ferroelectric ceramics. *Ferroelectrics*, 1995, **168**, 301–311.
25. Nuffer, J., Lupascu, D. C. and Rödel, J. Stability of pinning centers in fatigued lead-zirconate-titanate. *Appl. Phys. Lett.*, 2002, **80**(6), in press.
26. Salaneck, W. R., Some fatiguing effects in 8/65/35 PLZT fine grained ferroelectric ceramic. *Ferroelectrics*, 1972, **4**, 97–101.
27. Carl, K., Ferroelectric properties and fatiguing effects of modified $PbTiO_3$ ceramics. *Ferroelectrics*, 1975, **9**, 23–32.
28. Subbarao, E. C., Srikanth, V., Cao, W. and Cross, L. E., Domain switching and microcracking during poling of lead zirconate titanate ceramics. *Ferroelectrics*, 1993, **145**, 271–281.
29. Kim, S.-J. and Jiang, Q., Microcracking and electrical fatigue of polycrystalline ferroelectric ceramics. *Smart Mater. Struct.*, 1996, **5**, 321–326.
30. Nuffer, J., Lupascu, D. C. and Rödel, J., Microcrack clouds in fatigued electrostrictive 9. *5/65/35 PLZT*. *J. Eur. Ceram. Soc.*, 2001, **21**, 1421–1423.
31. Hill, M. D., White, G. S., Hwang, C.-S. and Lloyd, I. K., Cyclic damage in lead zirconate titanate. *J. Am. Ceram. Soc.*, 1996, **79**, 1915–1920.
32. Cao, H. and Evans, A. G., Electric-field-induced fatigue crack growth in piezoelectrics. *J. Am. Ceram. Soc.*, 1994, **77**, 1783–1786.
33. Nuffer, J., Lupascu, D. C. and Rödel, J., Acoustic emission in PZT under bipolar electric driving and uniaxial mechanical stress. *Ferroelectrics*, 2000, **240**, 27–36.
34. Pan, W., Yue, C. F. and Tosyali, O., Fatigue of ferroelectric polarization and the electric field induced strain in lead zirconate titanate ceramics. *J. Am. Ceram. Soc.*, 1992, **75**, 1534–1540.
35. Lucato, S., *LINCE (Linear Intercept Software)*. TU, Darmstadt, 1999.
36. Wroblewski, T., Clauβ, O., Crostack, H.-A., Ertel, B., Fandrich, F., Genzel, Ch., Hradil, K., Ternes, W. and Woldt, E., A new diffractometer for materials science and imaging at HASYLAB beamline G3. *Nucl. Instr. Meth. Phys. Res.*, 1999, **A428**, 570–582.
37. Weitzing, H., Schneider, G. A., Steffens, J., Hammer, M. and Hoffmann, M. J., Cyclic fatigue due to electric loading in ferroelectric ceramics. *J. Eur. Ceram. Soc.*, 1999, **19**, 1333–1337.
38. Smyth, D. M., Ionic transport in ferroelectrics. *Ferroelectrics*, 1994, **151**, 115–124.
39. Warren, W. L., Vanheusden, K., Dimos, D., Pike, G. E. and Tuttle, B. A., Oxygen vacancy motion in perovskite oxides. *J. Am. Ceram. Soc.*, 1996, **79**, 536–538.
40. Nuffer, L., Schroeder, M., Lupascu, D.C. and Rödel, J., Negligible oxygen liberation during bipolar electric cycling of ferroelectric PZT ceramics. Appl. Phys. Lett., (2001).
41. Becerro, A. I., McCammon, C., Langenhorst, F., Seifert, F. and Angel, R., Oxygen vacancy ordering in $CaTiO_3$ – $CaFeO_{2.5}$ perovskites: from isolated defects to infinite sheets. *Phase Transitions*, 1999, **69**, 133–146.
42. Slinkina, M. V., Dontsov, V. M. and Zhukovski, V. M., Diffusional penetration of silver from electrodes into PZT Ceramics. *J. Mater. Sci.*, 1993, **28**, 5189.
43. Nagata, H., Handeda, H., Sakaguchi, I., Takenaka, T. and Tanaka, T., Reaction and diffusion between PLZT ceramics and Ag electrode. *J. Ceram. Soc. Jpn.*, 1997, **105**, 862–867.
44. Kamiya, T., Tsurumi, T. and Daimon, M., Quantum calculations of molecular orbitals for PZT solid solutions by DUXα cluster method. In *Computer Aided Innovation of New Materials II*, ed.

M. Doyama, J. Kikara, M. Tanaka and R. Yamamoto. Elsevier Science Publisher B.V, Amsterdam, 1993.
45. Warren, W. L., Robertson Dimos, D. B., Tuttle, B. A. and Smyth, D. M., Transient hole traps in PZT. *Ferroelectrics*, 1994, **153**, 303–308.
46. Jiang, L. Z. and Sun, C. T., Crack growth behavior in piezoceramics under cyclic loads. *Ferroelectrics*, 1999, **233**, 211–223.
47. Lynch, C. S., Yang, W., Collier, L., Suo, Z. and McMeeking, R. M., Electric field induced cracking in ferroelectric ceramics. *Ferroelectrics*, 1995, **166**, 11–30.
48. Zimmermann, A., Hoffman, M., Flinn, B. D., Bordia, R. K., Chuang, T.-J., Fuller, E. R. and Rödel, J., Fracture of alumina with controlled pores. *J. Am. Ceram. Soc.*, 1998, **81**, 2449–2457.
49. Jiang, Q., Cao, W. and Cross, L. E., Electric fatigue in lead zirconate titanate ceramics. *J. Am. Ceram. Soc.*, 1994, **77**, 211–215.
50. Lupascu, D. C., Nuffer, J., Wallace, J. S. and Rödel, J., Role of crack formation in the electric fatigue behavior of ferroelectric PZT ceramics. In *Smart Structures and Materials 2000: Active Materials: Behavior and Mechanics*, SPIEVA-3492, ed. Christopher S. Lynch. 2000, pp. 209–216.